ACSNANO

www.acsnano.org

ARTICLE

Phase Diagram and Structure Map of Binary Nanoparticle Superlattices from a Lennard-Jones Model

Shang Ren, Yang Sun,* Feng Zhang,* Alex Travesset, Cai-Zhuang Wang, and Kai-Ming Ho

Cite This: *ACS Nano* 2020, 14, 6795−6802

Read Online

ACCESS | Metrics & More | Article Recommendations | Supporting Information

ABSTRACT: **A first-principles prediction of the binary nanoparticle phase diagram assembled by solvent evaporation has eluded theoretical approaches. In this paper, we show that a binary system interacting through the Lennard-Jones (LJ) potential contains all experimental phases in which nanoparticles are effectively described as quasi hard spheres. We report a phase diagram consisting of 53 equilibrium phases, whose stability is quite insensitive to the microscopic details of the potentials, thus giving rise to some type of universality. Furthermore, we show that binary lattices may be understood as consisting of certain particle clusters, *i.e.*, motifs, that provide a generalization of the four conventional Frank−Kasper polyhedral units. Our results show that metastable phases share the very same motifs as equilibrium phases. We discuss the connection with packing models, phase diagrams with repulsive potentials, and the prediction of likely experimental superlattices.**

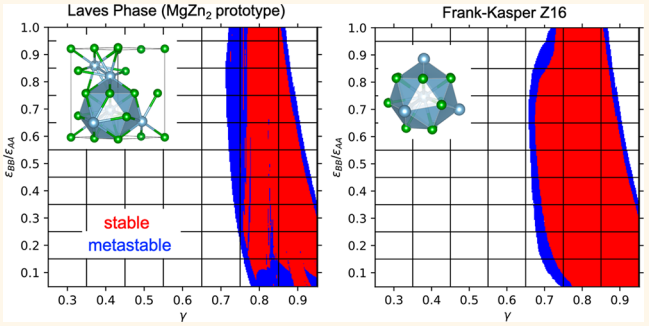

KEYWORDS: *nanoparticle, crystal gene, motif, material prediction, material design*

Compared with atoms, where size, shape, and bonding is completely fixed by the electronic structure, nanocrystals (NCs) offer a degree of tunability, as they can be synthesized with any size or shape and may be functionalized with a wide range of ligands,[1] which determine the bonding and play the same role as electrons in atomic crystals. Just binary NC systems, for example, form binary nanoparticle superlattices (BNSLs) and quasicrystals of extraordinary complexity.[2,3]

Early theoretical treatments described NCs as hard spheres (HS),[2] as a clear correlation was found between the maximum of the packing fraction and BNSL stability.[2,4] This correlation, however, was rather imperfect, as many experimental systems existed far from the maximum, implying low packing fraction, which would likely make those BNSLs unstable. Still, despite their limitations, HS models do provide a natural starting point to describe the equilibrium phases of NC systems: All experimentally reported BNSLs except Li_3Bi and $AuCu_3$[4,5] are thermodynamically stable at the peak of the packing fraction, where each NC is described as a (quasi)-HS.[5]

Strict HS models[6−13] thus play an important role in the prediction of BNSLs and NCs in general. In refs 14−16 it was shown that by allowing some compressibility or "softness", thus describing NCs as quasi-HS, the thermodynamic stability of the HS binary phases was enhanced and agreement with experiments improved. Based on the softer approximation, the orbifold topological model (OTM)[5,17] established the range of validity of the HS approximation, successfully describing all available experimental data as well as subsequent experiments[18] and simulations.[19−22] These calculations, however, only compared free energies for a set of predefined structures, and therefore, the question is how many phases would remain as stable or how many unknown ones would emerge under a general unrestricted structural search. Another important question is that those quasi-HS particles interact through a repulsive potential; thus it is necessary to appeal to the existence of some type of "universality" to translate those results into predictions for NC systems. Motivated by these considerations, in this paper we investigate quasi-HS models with attractive interactions. We will therefore use the genetic

Received: January 9, 2020
Accepted: June 1, 2020
Published: June 1, 2020

algorithm (GA)[23,24] to perform an open search in systems of Lennard-Jones (LJ) particles with additive interactions. We note that although this paper is motivated by systems in the nanoscale, the results are directly applicable to colloidal systems in the μ-range,[25,26] where NCs are well described by quasi-HS throughout.

Another important consideration toward a fully predictive theory for NC structure is the consideration that all experimental BNSLs reported to date can be described as arrangements of a small number of predefined particle clusters,[27] *i.e.*, motifs,[28] which generalize the four motifs (Z_{12}, Z_{14}, Z_{15}, Z_{16}) that describe Frank−Kasper (FK) phases.[29−32] We will therefore investigate the description of equilibrium and metastable structures as arising from a small subset of motifs as building blocks, not just as a way to construct all possible equilibrium lattices, but also to identify metastability and glassy or amorphous structures as systems arrested on their way to equilibrium.

MODEL

As a minimal model of attractive quasi-HS we consider an interaction between particles as described by the LJ potential:

$$U_{\mathrm{LJ}} = \begin{cases} 4\epsilon\left(\left(\frac{\sigma}{r}\right)^{12} - \left(\frac{\sigma}{r}\right)^{6}\right) & (r \le r_{\mathrm{cut}}) \\ 0 & (r > r_{\mathrm{cut}}) \end{cases} \quad (1)$$

We consider two types of particles, A and B, with the size of A larger than B ($\sigma_{AA} > \sigma_{BB}$). The interaction strength is such that $\epsilon_{AA} \ge \epsilon_{BB}$, which implements the well-documented requirement that the smaller the NCs,[19] the weaker the interaction. All calculations will be performed at $T = 0$, and therefore, the parameters $\epsilon_{AA} = 1$ and $\sigma_{AA} = 1$ are fixed without loss of generality. Then, the system becomes a function of $\gamma = \sigma_{BB}/\sigma_{AA}$, σ_{AB}, ϵ_{AB}, and ϵ_{BB}. We will further assume that interactions are additive so that the parameters are as follows:

$$\sigma_{AA} = 1.0 \qquad \epsilon_{AA} = 1.0$$

$$\sigma_{AB} = \frac{\sigma_{AA} + \sigma_{BB}}{2} = \frac{1+\gamma}{2} \qquad \epsilon_{AB} = \frac{\epsilon_{AA} + \epsilon_{BB}}{2} = \frac{1+\epsilon_{BB}}{2}$$

$$\sigma_{BB} = \gamma \qquad \epsilon_{BB} = \epsilon_{BB}$$

In this way, starting from six parameters (ϵ_{AA}, ϵ_{BB}, ϵ_{AB}, σ_{AA}, σ_{AB}, σ_{BB}) the model is reduced to two free parameters (ϵ_{BB} and γ).

In addition, we introduce the third parameter to control the stoichiometry, which is denoted by x. The structures will be presented in the form A_xB_{1-x}. In our calculations γ is varied from 0.3 to 0.9 and ϵ_{BB} from 0.1 to 1.0. The step size for both of them is set to be 0.1. The stoichiometry values are listed in Table 1.

The LJ potential was cut off at a value r_{cut}, which was set to be 3.5 times the radius of the larger particle: $r_{\mathrm{cut}} = 3.5\sigma_{AA} = 3.5$. It has been shown that accurate values for thermodynamic quantities are sensitive to r_{cut}.[33] One should expect minor corrections on some phase boundaries as a function of the cutoff value, a point that will be elaborated further elsewhere.

RESULTS AND DISCUSSION

We first illustrate the method in some detail for the case $\epsilon_{BB} = 1.0$ and then present the general results. We also proceed to rigorously characterize the motifs and identify them in the lattice structures.

Table 1. Configuration of Stoichiometry in GA Search

x	n(A):n(B)
0.1	1:9, 2:18
0.143	1:6, 2:12
0.167	1:5, 2:10, 3:15
0.2	1:4, 2:8, 3:12, 4:16
0.25	1:3, 2:6, 3:9, 4:12, 5:15
0.333	1:2, 2:4, 3:6, 4:8, 5:10, 6:12
0.4	2:3, 4:6, 6:9, 8:12
0.5	1:1, 2:2, 3:3, 4:4, 5:5, 6:6, 7:7, 8:8, 9:9, 10:10
0.6	3:2. 6:4. 9:6, 12:8
0.667	2:1, 4:2, 6:3, 8:4, 10:5, 12:6
0.75	3:1, 6:2, 9:3, 12:4, 15:5
0.8	4:1, 8:2, 12:3, 16:4
0.833	5:1, 10:2, 15:3
0.857	6:1, 12:2
0.9	9:1, 18:2

In order to name the different phases, we searched the Material Project Database[34] to find a prototype isostructural phase and name the GA calculated lattice accordingly. If no match is found, then we name the phase according to the following convention:

$$\mathrm{A}_m\mathrm{B}_{n\,\mathrm{identifier}}^{\mathrm{space\ group}} \quad (2)$$

Here m and n are the number of A and B particles within the unit cell. The space group is determined using the FINDSYM package,[35] with the tolerance for lattice and atomic positions set to 0.05. The identifier is necessary, as multiple phases with the same stoichiometry and space group, differing only in Wyckoff number and positions, are found.

The Case $\epsilon_{BB} = 1.0$. Here we consider $\epsilon_{BB} = \epsilon_{AA} = 1.0$, while $0.3 \le \gamma \le 0.9$. We first compute the energy of the ground state for the pure A and B states, which previous calculations[33,36] have shown to be the hcp phase. Here, however, because of the finite cutoff of LJ potentials, the fcc phase has lower energy. The identification of equilibrium phases proceeds by comparing their energy against phase separation into pure A and B. Then, out of this list of putative binary phases that are stable against phase separation, the energies are compared to establish the resulting true phase diagram equilibrium. This is how the phase diagram in Figure 1 is built, where there is only one stable BNSL, the $MgZn_2$ Frank−Kasper phase at $\gamma = 0.8$. We should note that the maximum of the packing fraction for this phase occurs for $\gamma_c = \sqrt{2/3} = 0.8165$,[5] which is very close.

Since it is common that structures that are metastable at 0 K can be observed in experiments at finite temperatures, we also considered metastable phases defined to be those within 0.1ϵ/particle in energy above the convex hull. As shown in Figure 1, there are a number of metastable phases at $x = 0.333$, which are minor variations of $MgZn_2$, as we analyze further below in the context of motifs.

General ϵ_{BB}. On physical grounds, it is expected that the smaller the particle, the weaker the interaction; hence we consider $\epsilon_{BB} \le 1$. In Figure 2, we provide a typical calculation for fixed $\gamma = 0.6$ as a function of both ϵ_{BB} and x. As expected (see Figure 1), the phase diagram is trivial for $\epsilon_{BB} = 1$. However, three phases, $TiCu_3$, AlB_2, and CrB, at $x = 0.25$, 0.333, and 0.5 are found for $\epsilon_{BB} = 0.8$.

https://dx.doi.org/10.1021/acsnano.0c00250
ACS Nano 2020, 14, 6795−6802

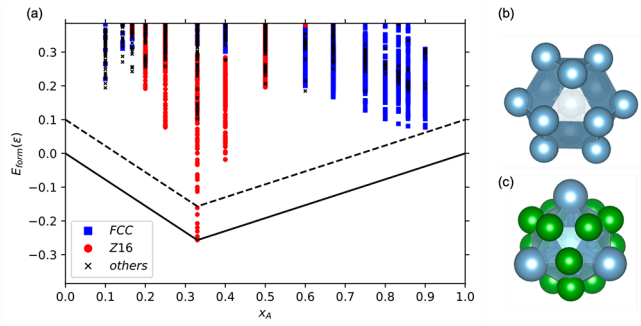

Figure 1. Structures searched by GA in ϵ_{BB} = 1.0 and γ = 0.8. (a) Formation energies (E_{form}) of structures searched by GA as a function of stoichiometry (x). Each point corresponds to a structure. The color of points are assigned by the type of motifs in the corresponding structure. The black solid line is the convex hull of the system, while the black dashed line is the threshold for metastable structures. (b) Structure of the FCC motif. (c) Structure of the $MgZn_2$ motif, which is Frank–Kasper Z_{16}.

By repeating the calculations shown in Figure 2 for the other values of ϵ_{BB} at a fixed γ = 0.6 (see Table 1), we constructed the phase diagram shown in Figure 3. In Figure 3 we note the appearance of seven additional phases for ϵ_{BB} < 0.6 that could not be matched to any prototype: Detailed descriptions for these and all other equilibrium phases are collected in Supporting Information Table S1. A database for all the structures is included in the Supporting Information.

Similarly, the phase diagrams for all other values of γ are also presented in Supporting Information Figure S2. Common to all these phase diagrams is the appearance of many diffusionless (martensitic), usually incongruent transformations, as a function of the energy parameter $\epsilon_{BB}/\epsilon_{AA}$. In Supporting Information Figure S3, we have also included phase diagrams for all values of $\epsilon_{BB}/\epsilon_{AA}$ in x and γ.

Motifs. We define motifs as the polyhedron consisting of a center particle and its first-shell neighbors. The motifs are generated according to the analysis of the bond length table from neighboring particles to the center (see details in Supporting Information Figure S6). In this study, we include only motifs with the larger A particles as the center. We will name motifs according to

$$\text{Motif} - \text{CN} - \text{Identifier} \quad (3)$$

where CN is the coordination (the number of particles) and identifier discriminates among motifs with the same coordination number.

We identified 187 equilibrium and 102 822 metastable structures. Out of the 187 equilibrium structures, we removed redundancies by a cluster alignment algorithm,[28,37] leading to only 53 equilibrium structures. Out of these 53 structures, we identified 42 motifs, which are listed in the order of increasing CN in Supporting Information Figure S4. A total of 416 391 motifs can be found in the 102 822 metastable structures. Among them, a vast majority (312 891) of the motifs of the metastable structures also exist in the equilibrium phases. In Table 2, we list the name, CN, and the percentage fraction of the 10 most frequent motifs present in metastable structures. Note that these 10 already account for more than 95% of the 312 891 motifs. The details about how to identify the motif from a crystal and how to identify if a crystal has the motif inside have been included in the Supporting Information.

As an illustrative example, we consider the case of ϵ_{BB} = 1 and γ = 0.8, where in Figure 1 we have shown the two relevant motifs are the fcc and the Frank–Kasper Z_{16}. By coloring each structure according to the motif, we can confirm that the metastable phases (all in red) have motifs that are small variations of the Frank–Kasper Z_{16} and that the vast majority of the structures found in other searches have motifs that are variations of either FCC or Frank–Kasper Z_{16}.

In Figure 4 we show the domain of stability and metastability for the $MgZn_2$ phase and the Z_{16} motif. The GA searches were performed on a mesh of γ and ϵ_{BB} with an increment of 0.1. Here, to improve the resolution of the stability range, we examined the stability of all GA-found structures and motifs on a finer mesh in the γ–ϵ_{BB} plane with an increment of 0.02. Rather interestingly, the stability range of the Z_{16} motif is larger than that of the $MgZn_2$ phase, indicating this motif is not unique to $MgZn_2$, but shared by other Laves and Frank–Kasper phases. Similar plots for the four more frequent motifs are shown in Figure 5.

Quite generally, the motifs are far more sensitive to γ than they are to $\epsilon_{BB}/\epsilon_{AA}$, confirming that the particle size is more important than the actual intensity of the interactions. It is consistent with all calculations that stable structures with the same values of γ tend to share motifs. As found for $MgZn_2$ and Z_{16}, the regions for stability and metastability are wider than the corresponding structures, thus indicating that motifs define very general families of structures, like Laves phases. A

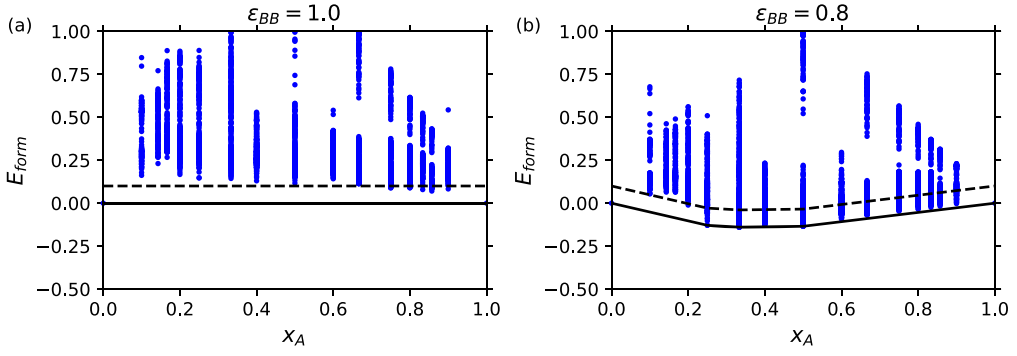

Figure 2. Two examples of GA results for γ = 0.6. In each figure, the solid line is the convex hull, while the dashed line is the threshold for metastable structures; see the discussion above. (a) Structures searched by GA as a function of x when ϵ_{BB} = 1.0: There are no stable binary structures between x = 0 and x = 1. (b) Structures searched by GA as a function of x for ϵ_{BB} = 0.8. There are three stable structures, which appear at x = 0.25 ($TiCu_3$), x = 0.333 (AlB_2), and x = 0.5 (CrB).

https://dx.doi.org/10.1021/acsnano.0c00250
ACS Nano 2020, 14, 6795–6802

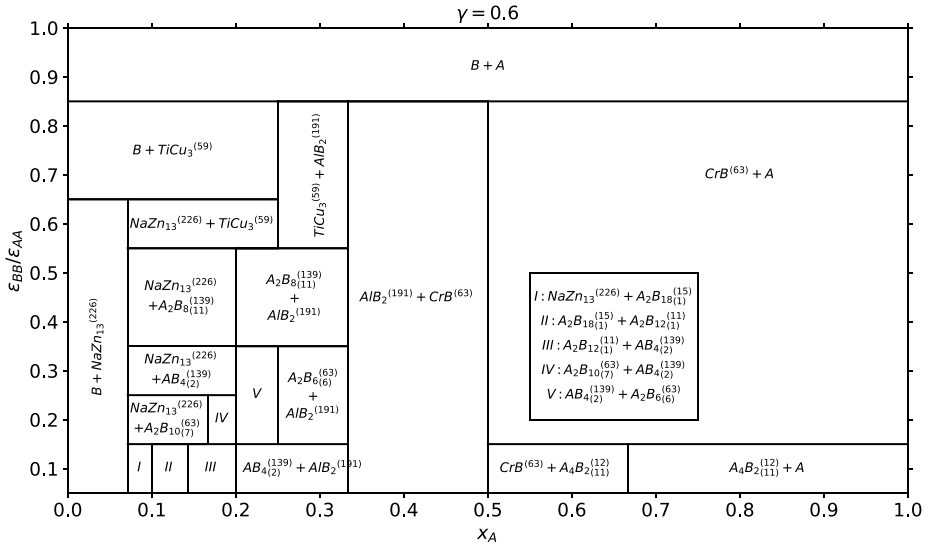

Figure 3. Phase diagram in x and $\epsilon_{BB}/\epsilon_{AA}$ for $\gamma = 0.6$.

Table 2. Ten Most Frequent Motifs in Metastable Structures

motif	CN	frequency
fcc	12	31.4%
hcp	12	18.9%
octahedron (motif-6-4)	6	9.8%
half hexagonal prism 1 (motif-6-2)	6	9.1%
triangular prism (motif-6-3)	6	6.4%
half hexagonal prism 2 (motif-6-1)	6	5.3%
bcc	8	5.0%
hexagonal prism (motif-12-3)	12	4.8%
half truncated cube (motif-12-1)	12	2.3%
MoB (motif-13-1)	13	2.2%
total		95%

classification of motifs by renormalized angle sequences[38,39] has been included in the Supporting Information.

This study has identified 53 equilibrium lattices and 42 motifs (with the larger particle A as reference). We now discuss the relevance of these results for packing models,[8,10] their connection to the motifs reported in quasi-Frank–Kasper phases,[17] and their implications for binary superlattices.

Packing Phase Diagram. We consider the study of Hopkins *et al.*[10] as the reference phase diagram for packing problems, although it includes only unit cells containing up to 12 particles. Consistently with this study we concentrate on the range $0.3 \leq \gamma \leq 1$, also because for smaller γ there are many phases with narrow stability ranges that are less relevant in actual experimental systems.

From Table 3, the packing of the binary phase diagram contains 13 phases for the $0.3 \leq \gamma \leq 1$ range. For large $\gamma > 0.528$ only two phases exist, AlB_2 and A_3B, which are both found in binary LJ systems (if allowing for small differences in A_3B). For $0.488 < \gamma < 0.528$, however, the $AuTe_2$ phase is reported; we did not find such a phase, but we do report the motif-6-2 as stable for the same range of γ (see Supporting Information), which is present in the equilibrium phases at $\gamma = 0.5$ $A_4B_6^{(166)}_{(9)}$, BaCu, and TePt. Some other phases, which are reported as packing phases[10] but not stable in the GA search, are also identified to have the motif in the corresponding γ

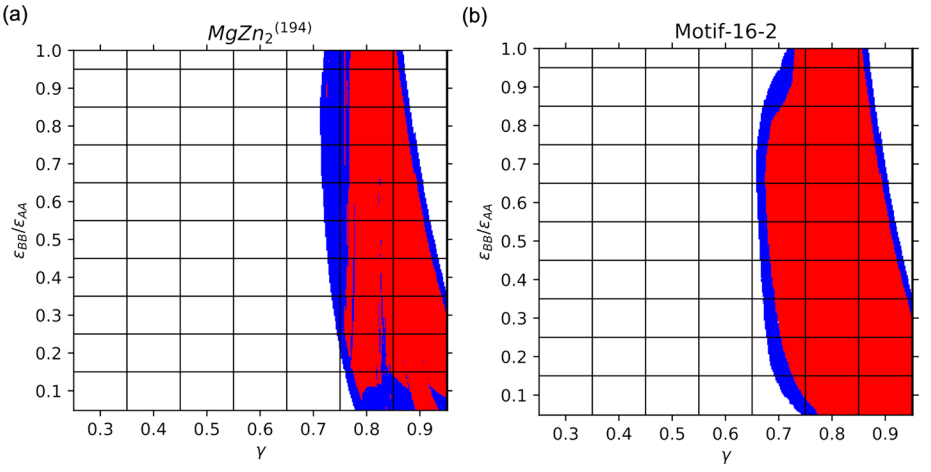

Figure 4. (a) Map of $MgZn_2$ in γ and ϵ_{BB}. The red regime indicates that the structure of $MgZn_2$ is thermodynamically stable, while in the blue regime it is metastable. (b) Map for the Z_{16} motif with red stable, blue metastable. The red regime is where the stable structure has a Z_{16} motif inside. Note that the motif has a wider range of both stability and metastability, as it also appears in other Laves phase, such as the $MgCu_2$ and $MgNi_2$.

https://dx.doi.org/10.1021/acsnano.0c00250
ACS Nano 2020, 14, 6795–6802

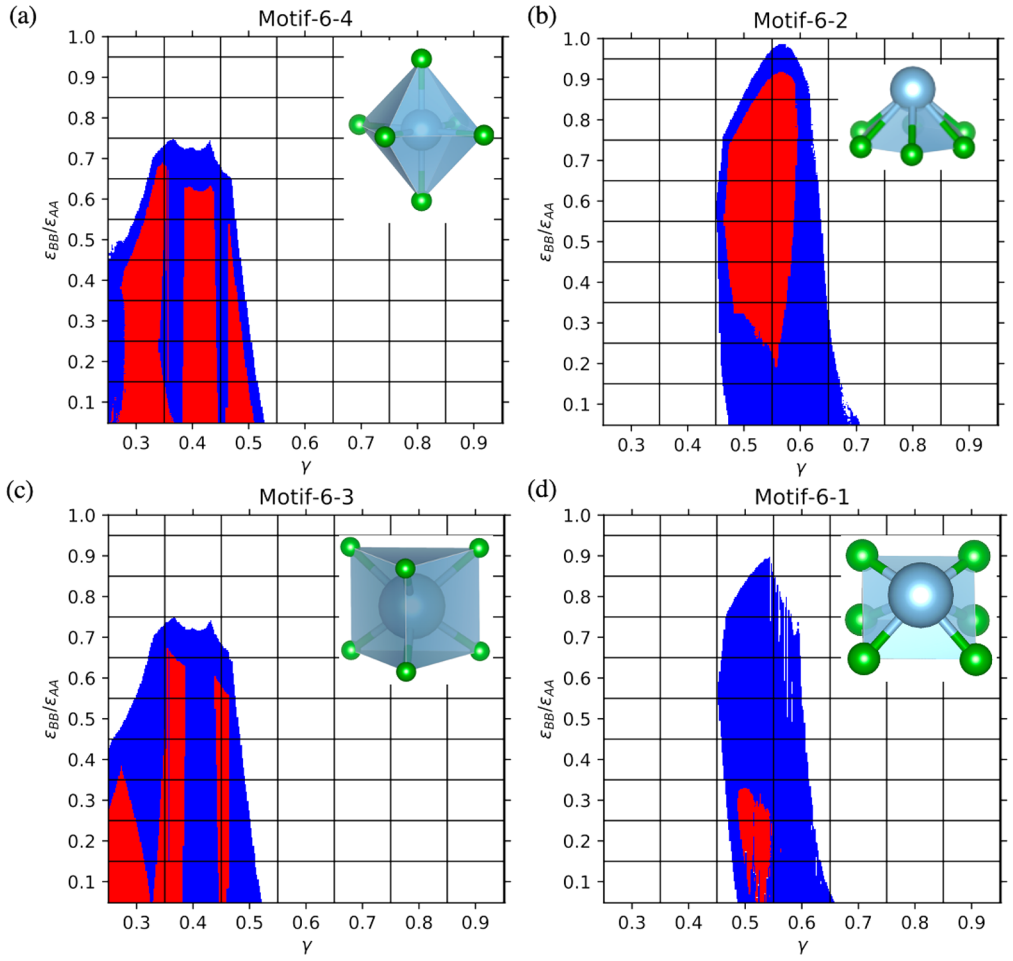

Figure 5. Map for first four frequent motifs in γ and ϵ_{BB} excludes the general motif fcc and hcp. (a) Octahedron; (b) half hexagonal prism 1; (c) triangular prism; (d) half hexagonal prism 2. Red indicates stable structures, and blue indicates metastable.

Table 3. Comparison between Packing Phases[10] and Our Study for $0.3 \leq \gamma \leq 1$[a]

phase	γ-range	ref	SG	LJ	distortion
A_3B	[0.618, 0.660]	40	59	$TiCu_3$	
AlB_2	[0.528, 0.620]		191	AlB_2	
$AuTe_2$	[0.488, 0.528]	8	12	motif-6-2	
(2−2)*	[0.480, 0.497]	41	11	motif-6-1	
(4−2)	[0.488, 0.483]	10	191	motif-12-3	
(5−2)	[0.480, 0.483]	10	44		
(7−3)	[0.468, 0.480]	10	71	motif-12-3	
$HgBr_2$	[0.443, 0.468]	8	36	motif-6-4	
(6−6)	[0.414, 0.457]	10	11	motif-6-4	
XY	[0.275, 0.414]	10			
$(6,1)_4$	[0.352, 0.321]	10	69	$A_2B_{12(1)}^{(139)}$	*
$(6,1)_6$	[0.321, 0.304]	10	139	$A_2B_{12(1)}^{(139)}$	*
$(6,1)_8$	[0.302, 0.292]	10	139	$A_2B_{12(1)}^{(139)}$	*

[a]SG = space group. The * indicates there are small distortions in the LJ phase, compared with the packing phase. Motifs in the LJ column indicate that they are not stable in the GA result, but they have the motif inside in the corresponding γ regime.

regime. This indicates that these packing phases may be metastable in our calculation. For smaller γ, there is also overlap if allowing for small distortions.

Other phases that have large packing fractions, such as CrB and S74e/h (KHg_2 in our notation),[8] that are metastable in the packing phase diagram attain equilibrium, thus showing that the LJ system augments the number of stable phases as compared with packing models.

Motifs and Quasi-Frank−Kasper Phases. In ref 17 it was shown that all experimental BNSLs could be described as disclinations of the {3, 3, 5} polytope, thus generalizing four well-known Frank−Kasper motifs, Z_{12}, Z_{14}, Z_{15}, Z_{16},[29,30] to include other motifs.

In Table 4 we show the equivalence between quasi-Frank−Kasper motifs and the ones obtained in this work, which include only those with the A particle as reference. It should be pointed that the motifs are not completely the same, as in ref 17 the motifs were defined by the Voronoi cell and its corresponding neighbors, which is a slightly different definition than the one used in this paper.

Table 4. Motifs in Quasi-Frank−Kasper Phases[17] Compared to the Ones Described in This Work

QFK[17]	Z_6	Z_{12}''	Z_{14}'	Z_{16}	Z_{18}''	Z_{24}
this work	motif-6-4	motif-12-2	motif-14-1	motif-16-2	motif-18-3	motif-24-1 or motif-24-3

https://dx.doi.org/10.1021/acsnano.0c00250
ACS Nano 2020, 14, 6795−6802

Experimental Results. The list of experimentally reported BNSLs is taken from ref 5, where we have excluded two-dimensional superlattices and those where nanocrystals cannot be approximated as spherical; see ref 3. The comparison between the results obtained in this paper and experimental BNSLs is provided in Table 5.

Table 5. Experimentally Determined Structures[a]

experiment		binary LJ		
BNSL	γ-range		γ-range	ϵ_{BB}-range
NaCl	[0.41, 0.60]		[0.2, 0.5]	[0.1, 0.8]
CsCl	[0.71, 0.90]	NF		
AuCu	[0.58, 0.71]	NF		
DDQC/AT	[0.41, 0.43]	NA		
AlB_2	[0.45, 0.70]		[0.4, 0.7]	[0.1, 0.9]
$MgZn_2$	[0.60, 0.81]		[0.7, 1.0]	[0.1, 1.0]
$AuCu_3$	[0.40, 0.60]	NF		
Li_3Bi	[0.53, 0.56]	NF		
Fe_4C	[0.55, 0.65]	NF		
$CaCu_5$	[0.60, 0.80]		[0.6, 0.8]	[0.1, 0.9]
CaB_6	[0.43, 0.47]		[0.3, 0.5]	[0.1, 0.8]
$bccAB_6$	[0.45, 0.50]		[0.4, 0.6]	[0.1, 0.5]
$cubAB_{13}$	[0.55, 0.60]	NF		
$NaZn_{13}$	[0.47, 0.70]		[0.6]	[0.1, 0.6]

[a]NA: Phase not available in this study. NF: Phase not found in this study. The DDQC/AT is a quasicrystal phase. The $bccAB_6$ phase is also known as $C_{60}K_6$ and is denoted as $AB_{6(1)}^{(229)}$ in this paper.

Seven of the experimentally reported BNSLs, namely, NaCl, AlB_2, $MgZn_2$, $CaCu_5$, CaB_6, $bccAB_6$, and $NaZn_{13}$, are found as equilibrium phases in the LJ system essentially for the same range of γ. The fact that in our results the stability is roughly independent of ϵ_{BB} in certain regions provides some support for the idea that microscopic details of the potential are unimportant in this region ("universality"). Further making this point is that the same phases are stable for soft repulsive potentials in the same γ-range.[14−16]

We now analyze the phases reported in experiments that are not in equilibrium in our study. One of them is beyond the scope of our calculation: DDQC/AT, which is a quasicrystal. The Li_3Bi and also the $AuCu_3$ are stabilized by large deformations of the ligands, *i.e.* vortices,[17] and therefore are not possible to obtain from a quasi-HS approximation. The Fe_4C phase was observed in 2006,[42] and since then, it has not been reported in any further study, which may suggest it is metastable, and furthermore, it can only be stabilized by vortices.[5] The CsCl phase has a very narrow range of stability around $\gamma_c = \sqrt{3} - 1 = 0.732$,[5] which is likely missed by the discretization of γ values in our study. Finally, AuCu occurs when there is ligand loss[17,43] and is stabilized through a different mechanism involving the nonspherical shape of the nanocrystal. We therefore conclude that the binary LJ model successfully predicts those experimentally reported phases that can be described as quasi-hard spheres. This is in contrast to packing models, where $MgZn_2$ or $CaCu_5$ phases, widely reported in experiments, are not equilibrium phases (maximum of the packing fractions). See Figure 6 for a visual summary of this discussion.

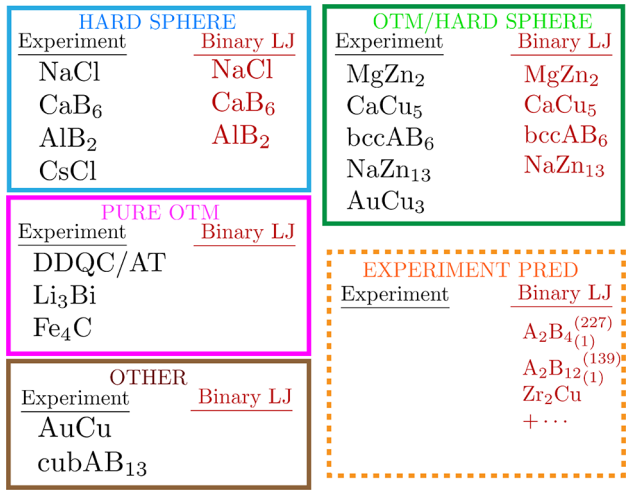

Figure 6. Summary of the main results of the paper: The experimental phases are classified according to hard sphere, OTM/hard sphere (exists when NCs are modeled as hard spheres but are stabilized by vortices),[17] pure OTM (only stable with vortices), and other (observed in special cases, such as ligand detachment[43]). See also Table 5. Consistent with the LJ assumptions, only the hard sphere phases are found in our work. The Experiment Pred includes those strong candidates to be found experimentally, as discussed below.

CONCLUSIONS

By the use of genetic algorithm, we have been able to predict stable structures under different sizes of particles and strengths of interaction ($\gamma \in [0.3 \text{ to } 0.9]$, $\epsilon_{BB} \in [0.1 \text{ to } 1.0]$). We report 53 stable phases, which cover a significant part of currently reported structures. Besides that, we also predict 35 stable structures which are not in the Material Project database. We find that the type of stable structures strongly depends on γ, but weakly on $\epsilon_{BB} < 1$, providing evidence that the stability of the lattices has a weak dependence on the potential details (universality). By comparing our results with other theoretical and experimental works, it is shown that regardless of potential details, the same γ regime has the same stable structure, which reinforces that the stable structure has a weak dependence on the potential details.

There are two aspects about the limitations of the hard sphere description: The first is that it does *not* provide a free energy: the observed phases are not the ones with maximum packing fraction,[10] but rather, ones where the packing fraction is maximum for the particular structure. This is where the binary LJ becomes important: the stable phases are the ones that minimize the free energy (modeled as the LJ potential). The second limitation is that it does not model large deformations of the ligand shell: these cases go beyond the LJ model and are evident from Figure 6, showing that these phases are absent.

The crystalline motifs are employed to describe the large amount of metastable structures. We find that metastable structures mostly can be described from the motifs present in equilibrium structures, thus suggesting the possibility of building superlattices by patching all motifs that can tile the 3D space, as similarly done in the more restricted case of Frank−Kasper phases.[44] It also raises the possibility of motifs being present within the liquid[11] as a way to anticipate the emergent crystalline structure.

https://dx.doi.org/10.1021/acsnano.0c00250
ACS Nano 2020, 14, 6795−6802

Comparing with available experimental results (see Table 5 and Figure 6), the binary LJ model captures all the equilibrium phases where nanocrystals can be faithfully described as quasi hard spheres: NaCl, AlB_2, $MgZn_2$, $CaCu_5$, CaB_6, bccAB$_6$, and $NaZn_{13}$. The other phases reported in experiments either require the presence of vortices, as predicted by the OTM,[5,17] or are stable over a very narrow range of γ values, likely missed by the necessary discrete number considered in our study.

Packing phase diagram models reported 14 equilibrium phases in the interval $\gamma \in [0.3, 1)$ (see Table 3), while our study reports 53, thus showing that binary LJ systems have a more complex phase diagram. Rather interestingly, phases such as $MgZn_2$ or $CaCu_5$, which are very common in experiments, are absent in the packing phase diagram. Although very useful in identifying at which γ values a phase is likely to appear, packing models give very poor predictions on which, among all possible phases, will actually be observed.

The two guiding principles for stability of BNSLs in experiments are high packing fraction (or low Lennard-Jones energy) and tendency toward icosahedral order, as reflected in the motifs.[5,18] Therefore, we expect that those equilibrium Lennard-Jones phases with quasi-Frank-Kasper motifs, for example, the BNSLs $A_2B_{4(1)}^{(227)}$ and $A_2B_{12(1)}^{(139)}$ (motif-16-2) or $Zr_2Cu_{(1)}^{(139)}$ (motif-14-1), will be excellent candidates to search for BNSLs; see Figure 6. Definitely, these ideas will be developed further in the near future, where the 53 stable lattices will be studied with more realistic nanocrystal models described at the atomic level.

In this work we focused on spherically symmetric potentials with additive interactions, as described by relations like

$$\epsilon_{AB} = \frac{1}{2}(\epsilon_{AA} + \epsilon_{BB}) \quad (4)$$

It is of interest to consider more general models, where these restrictions are lifted. This, however, will be the subject of another study.

METHODS

The crystal structure searches with GA were constrained only by stoichiometry, without any assumption on the Bravais lattice type, symmetry, atom basis, or unit cell dimensions (up to a maximum of particles per unit cell). During the GA search, energy was used as the only criteria for optimizing the candidate pool. At each GA generation, 64 structures are generated from the parent structure pool *via* the mating procedure described in refs 23, 24, and 45. The mating process was based on real-space "cut-and-paste" operations that were first introduced to optimize cluster structures.[23] This process was extended to predict low-energy crystal structures by Oganov[45] and reviewed in ref 24. Here, we follow the same procedure that was described in detail in ref 24 and was implemented in the Adaptive Genetic Algorithm software.

With a given set of LJ parameters, we performed three GA searches independently, with each GA search running for 1000 generations. The maximum number of particles per unit cell used in each search was 20, and thus, phases with large unit cells, the most relevant being $NaZn_{13}$, could not be included. Therefore, we include $NaZn_{13}$ into our calculation manually. All energy calculations and structure minimizations were performed by the LAMMPS code[46] with some cross checks using HOOMD-Blue[47] with FIRE minimization.[48] The database of binary lattices in HOODLT[33] was also used.

ASSOCIATED CONTENT

Supporting Information

The Supporting Information is available free of charge at https://pubs.acs.org/doi/10.1021/acsnano.0c00250.

List and maps of structures searched by the genetic algorithm; phase diagrams of equilibrium structures; equilibrium motif database; maps of motifs; algorithms for motif identification and renormalized angle sequence (PDF)

AUTHOR INFORMATION

Corresponding Authors

Yang Sun − *Department of Physics and Astronomy, Iowa State University, Ames, Iowa 50011, United States; Ames Laboratory, Ames, Iowa 50011, United States; Department of Applied Physics and Applied Mathematics, Columbia University, New York, New York 10027, United States;* orcid.org/0000-0002-4344-2920; Email: ys3339@columbia.edu

Feng Zhang − *Ames Laboratory, Ames, Iowa 50011, United States*; Email: fzhang@ameslab.gov

Authors

Shang Ren − *Department of Physics and Astronomy, Iowa State University, Ames, Iowa 50011, United States; Ames Laboratory, Ames, Iowa 50011, United States;* orcid.org/0000-0001-6904-7737

Alex Travesset − *Department of Physics and Astronomy, Iowa State University, Ames, Iowa 50011, United States; Ames Laboratory, Ames, Iowa 50011, United States;* orcid.org/0000-0001-7030-9570

Cai-Zhuang Wang − *Department of Physics and Astronomy, Iowa State University, Ames, Iowa 50011, United States; Ames Laboratory, Ames, Iowa 50011, United States;* orcid.org/0000-0002-0269-4785

Kai-Ming Ho − *Department of Physics and Astronomy, Iowa State University, Ames, Iowa 50011, United States; Ames Laboratory, Ames, Iowa 50011, United States*

Complete contact information is available at: https://pubs.acs.org/10.1021/acsnano.0c00250

Notes

The authors declare no competing financial interest.

ACKNOWLEDGMENTS

A.T. acknowledges discussions with I. Coropceanu and D. Talapin. We also thank Prof. Torquato for facilitating the data of his group packing studies. Work at Ames Laboratory was supported by the U.S. Department of Energy, Basic Energy Sciences, Materials Science and Engineering Division, under Contract No. DE-AC02-07CH11358, including a grant of computer time at the National Energy Research Supercomputing Center (NERSC) in Berkeley, CA. The Laboratory Directed Research and Development (LDRD) program of Ames Laboratory supported the use of GPU-accelerated computing. Y.S. was partially supported by National Science Foundation awards EAR-1918134 and EAR-1918126.

REFERENCES

(1) Kovalenko, M. V.; Manna, L.; Cabot, A.; Hens, Z.; Talapin, D. V.; Kagan, C. R.; Klimov, V. I.; Rogach, A. L.; Reiss, P.; Milliron, D. J.; Guyot-Sionnnest, P.; Konstantatos, G.; Parak, W. J.; Hyeon, T.; Korgel, B. A.; Murray, C. B.; Heiss, W. Prospects of Nanoscience with Nanocrystals. *ACS Nano* **2015**, *9*, 1012−1057.

(2) Shevchenko, E. V.; Talapin, D. V.; O'Brien, S.; Murray, C. B. Polymorphism in AB13 Nanoparticle Superlattices: An Example of Semiconductor-Metal Metamaterials. *J. Am. Chem. Soc.* **2005**, *127*, 8741−8747.

(3) Boles, M. A.; Engel, M.; Talapin, D. V. Self-Assembly of Colloidal Nanocrystals: From Intricate Structures to Functional Materials. *Chem. Rev.* **2016**, *116*, 11220−11289.
(4) Boles, M. A.; Talapin, D. V. Many-Body Effects in Nanocrystal Superlattices: Departure from Sphere Packing Explains Stability of Binary Phases. *J. Am. Chem. Soc.* **2015**, *137*, 4494−4502.
(5) Travesset, A. Soft Skyrmions, Spontaneous Valence and Selection Rules in Nanoparticle Superlattices. *ACS Nano* **2017**, *11*, 5375−5382.
(6) Eldridge, M. D.; Madden, P. A.; Frenkel, D. Entropy-Driven Formation of a Superlattice in a Hard-Sphere Binary Mixture. *Nature* **1993**, *365*, 35−37.
(7) Kummerfeld, J. K.; Hudson, T. S.; Harrowell, P. The Densest Packing of AB Binary Hard-Sphere Homogeneous Compounds across All Size Ratios. *J. Phys. Chem. B* **2008**, *112*, 10773−10776.
(8) Filion, L.; Dijkstra, M. Prediction of Binary Hard-Sphere Crystal Structures. *Phys. Rev. E* **2009**, *79*, 46714.
(9) Filion, L.; Marechal, M.; van Oorschot, B.; Pelt, D.; Smallenburg, F.; Dijkstra, M. Efficient Method for Predicting Crystal Structures at Finite Temperature: Variable Box Shape Simulations. *Phys. Rev. Lett.* **2009**, *103*, 188302.
(10) Hopkins, A. B.; Stillinger, F. H.; Torquato, S. Densest Binary Sphere Packings. *Phys. Rev. E* **2012**, *85*, 21130.
(11) Damasceno, P. F.; Engel, M.; Glotzer, S. C. Predictive Self-Assembly of Polyhedra into Complex Structures. *Science* **2012**, *337*, 453−457.
(12) Torquato, S. Perspective: Basic Understanding of Condensed Phases of Matter *via* Packing Models. *J. Chem. Phys.* **2018**, *149*, 43−46.
(13) Cersonsky, R. K.; van Anders, G.; Dodd, P. M.; Glotzer, S. C. Relevance of Packing to Colloidal Self-Assembly. *Proc. Natl. Acad. Sci. U. S. A.* **2018**, *115*, 1439.
(14) Travesset, A. Binary Nanoparticle Superlattices of Soft-Particle Systems. *Proc. Natl. Acad. Sci. U. S. A.* **2015**, *112*, 9563−9567.
(15) Horst, N.; Travesset, A. Prediction of Binary Nanoparticle Superlattices from Soft Potentials. *J. Chem. Phys.* **2016**, *144*, No. 014502.
(16) LaCour, R. A.; Adorf, C. S.; Dshemuchadse, J.; Glotzer, S. C. Influence of Softness on the Stability of Binary Colloidal Crystals. *ACS Nano* **2019**, *13*, 13829−13842.
(17) Travesset, A. Nanoparticle Superlattices as Quasi-Frank-Kasper Phases. *Phys. Rev. Lett.* **2017**, *119*, 1−5.
(18) Coropceanu, I.; Boles, M. A.; Talapin, D. V. Systematic Mapping of Binary Nanocrystal Superlattices: The Role of Topology in Phase Selection. *J. Am. Chem. Soc.* **2019**, *141*, 5728−5740.
(19) Waltmann, C.; Horst, N.; Travesset, A. Capping Ligand Vortices as "Atomic Orbitals" in Nanocrystal Self-Assembly. *ACS Nano* **2017**, *11*, 11273−11282.
(20) Waltmann, T.; Waltmann, C.; Horst, N.; Travesset, A. Many Body Effects and Icosahedral Order in Superlattice Self-Assembly. *J. Am. Chem. Soc.* **2018**, *140*, 8236−8245.
(21) Waltmann, C.; Horst, N.; Travesset, A. Potential of Mean Force for Two Nanocrystals: Core Geometry and Size, Hydrocarbon Unsaturation, and Universality with Respect to the Force Field. *J. Chem. Phys.* **2018**, *149*, No. 034109.
(22) Zha, X.; Travesset, A. Stability and Free Energy of Nanocrystal Chains and Superlattices. *J. Phys. Chem. C* **2018**, *122*, 23153−23164.
(23) Deaven, D. M.; Ho, K. M. Molecular Geometry Optimization with a Genetic Algorithm. *Phys. Rev. Lett.* **1995**, *75*, 288−291.
(24) Ji, M.; Wang, C. Z.; Ho, K. M. Comparing Efficiencies of Genetic and Minima Hopping Algorithms for Crystal Structure Prediction. *Phys. Chem. Chem. Phys.* **2010**, *12*, 11617−11623.
(25) Sanders, J. V.; Murray, M. J. Ordered Arrangements of Spheres of Two Different Sizes in Opal. *Nature* **1978**, *275*, 201.
(26) Murray, M. J.; Sanders, J. V. Close-Packed Structures of Spheres of Two Different Sizes II. The Packing Densities of Likely Arrangements. *Philos. Mag. A* **1980**, *42*, 721−740.
(27) Travesset, A. Topological Structure Prediction in Binary Nanoparticle Superlattices. *Soft Matter* **2017**, *13*, 147−157.
(28) Sun, Y.; Zhang, F.; Ye, Z.; Zhang, Y.; Fang, X.; Ding, Z.; Wang, C. Z.; Mendelev, M. I.; Ott, R. T.; Kramer, M. J.; Ho, K. M. 'Crystal Genes' in Metallic Liquids and Glasses. *Sci. Rep.* **2016**, *6*, 23734.
(29) Frank, F. C.; Kasper, J. S. Complex Alloy Structures Regarded as Sphere Packings. I. Definitions and Basic Principles. *Acta Crystallogr.* **1958**, *11*, 184−190.
(30) Frank, F. C.; Kasper, J. S. Complex Alloy Structures Regarded as Sphere Packings. II. Analysis and Classification of Representative Structures. *Acta Crystallogr.* **1959**, *12*, 483−499.
(31) Kleman, M.; Sadoc, J. F. A Tentative Description of the Crystallography of Amorphous Solids. *J. Phys., Lett.* **1979**, *40*, 569−574.
(32) Nelson, D. R. Order, Frustration, and Defects in Liquids and Glasses. *Phys. Rev. B: Condens. Matter Mater. Phys.* **1983**, *28*, 5515−5535.
(33) Travesset, A. Phase Diagram of Power Law and Lennard-Jones Systems: Crystal Phases. *J. Chem. Phys.* **2014**, *141*, 164501.
(34) Jain, A.; Ong, S. P.; Hautier, G.; Chen, W.; Richards, W. D.; Dacek, S.; Cholia, S.; Gunter, D.; Skinner, D.; Ceder, G.; Persson, K. A. Commentary: The Materials Project: A Materials Genome Approach to Accelerating Materials Innovation. *APL Mater.* **2013**, *1*, 9901.
(35) Stokes, H. T.; Hatch, D. M. FINDSYm: Program for Identifying the Space-Group Symmetry of A Crystal. *J. Appl. Crystallogr.* **2005**, *38*, 237−238.
(36) Stillinger, F. H. Lattice Sums and Their Phase Diagram Implications for the Classical Lennard-Jones Model. *J. Chem. Phys.* **2001**, *115*, 5208−5212.
(37) Fang, X. W.; Wang, C. Z.; Yao, Y. X.; Ding, Z. J.; Ho, K. M. Atomistic Cluster Alignment Method for Local Order Mining in Liquids and Glasses. *Phys. Rev. B: Condens. Matter Mater. Phys.* **2010**, *82*, 184204.
(38) Lv, X.; Zhao, X.; Wu, S.; Wu, P.; Sun, Y.; Nguyen, M. C.; Shi, Y.; Lin, Z.; Wang, C.-Z.; Ho, K.-M. A Fe-P Network-Generation Scheme to Search for Low-Energy LiFePO4 Crystal Structures. *J. Mater. Chem. A* **2017**, *5*, 14611−14618.
(39) Lv, X.; Ye, Z.; Sun, Y.; Zhang, F.; Yang, L.; Lin, Z.; Wang, C. Z.; Ho, K. M. A Comparative Study of Sm Networks in Al-10 at.%Sm Glass and Associated Crystalline Phases. *Philos. Mag. Lett.* **2018**, *98*, 27−37.
(40) O'Toole, P. I.; Hudson, T. S. New High-Density Packings of Similarly Sized Binary Spheres. *J. Phys. Chem. C* **2011**, *115*, 19037−19040.
(41) Marshall, G. W.; Hudson, T. S. Dense Binary Sphere Packings. *Beitr. Algebra Geom.* **2010**, *51*, 337−344.
(42) Shevchenko, E. V.; Talapin, D. V.; Kotov, N. A.; O'Brien, S.; Murray, C. B. Structural Diversity in Binary Nanoparticle Superlattices. *Nature* **2006**, *439*, 55−59.
(43) Boles, M. A.; Talapin, D. V. Binary Assembly of PbS and Au Nanocrystals: Patchy PbS Surface Ligand Coverage Stabilizes the CuAu Superlattice. *ACS Nano* **2019**, *13*, 5375−5384.
(44) Dutour Sikirić, M.; Delgado-Friedrichs, O.; Deza, M. Space Fullerenes: A Computer Search for New Frank-Kasper Structures. *Acta Crystallogr., Sect. A: Found. Crystallogr.* **2010**, *A66*, 602−615.
(45) Oganov, A. R.; Glass, C. W. Crystal Structure Prediction Using *Ab Initio* Evolutionary Techniques: Principles and Applications. *J. Chem. Phys.* **2006**, *124*, 244704.
(46) Plimpton, S. Fast Parallel Algorithms for Short-Range Molecular Dynamics. *J. Comput. Phys.* **1995**, *117*, 1−19.
(47) Anderson, J. A.; Lorenz, C. D.; Travesset, A. General Purpose Molecular Dynamics Simulations Fully Implemented on Graphics Processing Units. *J. Comput. Phys.* **2008**, *227*, 5342−5359.
(48) Bitzek, E.; Koskinen, P.; Gähler, F.; Moseler, M.; Gumbsch, P. Structural Relaxation Made Simple. *Phys. Rev. Lett.* **2006**, *97*, 170201.

https://dx.doi.org/10.1021/acsnano.0c00250
ACS Nano 2020, 14, 6795−6802